

Supplementary Material to

“CO₂-selective methanol steam reforming on In-doped Pd studied by ambient-pressure X-ray Photoelectron Spectroscopy“

Christoph Rameshan^{a,b}, Harald Lorenz^a, Lukas Mayr^a, Simon Penner^{a,*}, Dmitry Zemlyanov^c, Rosa Arrigo^b, Michael Haevecker^b, Raoul Blume^b, Axel Knop-Gericke^b, Robert Schlögl^b,

Bernhard Klötzer^a

^aInstitute of Physical Chemistry, University of Innsbruck, Innrain 52a, A-6020 Innsbruck, Austria

^bDepartment of Inorganic Chemistry, Fritz-Haber-Institute of the Max-Planck-Society, Faradayweg 4–6, D-14195 Berlin, Germany

^cPurdue University, Birck Nanotechnology Center, 1205 West State Street, West Lafayette, IN 47907-2057, USA

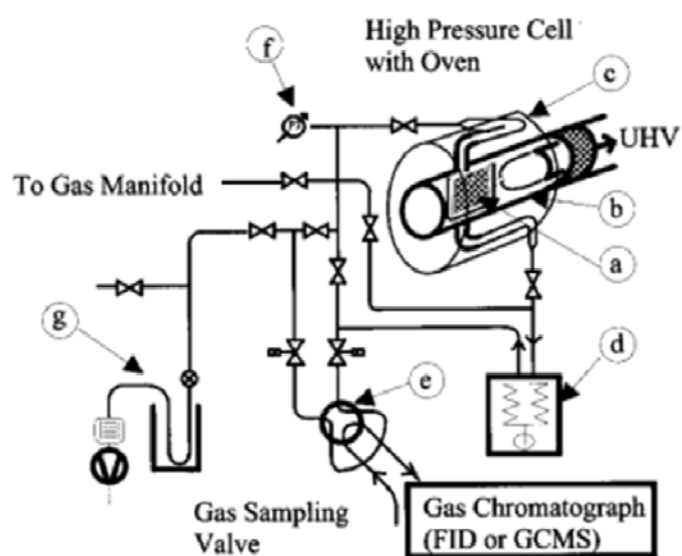


FIG. S1: Schematic of the high pressure cell: (a) catalyst sample in the glass frame, (b) Pyrex glass reaction cell, (c) oven, (d) circulation pump, (e) sample loop valve, (f) pressure transducer, (g) liquid nitrogen trap and rotary pump.

Fig. S1: detailed description/photograph of high-pressure reaction cell setup as derived from

[1]:

Ad Fig.S1: The reactor and the connecting glass tubes consist of Pyrex glass. The reactor is heated from the outside by an oven mounted on a linear motion car and the temperature is monitored with a thermocouple pressed against the outer front side of the reactor by a spring and regulated by a proportional integral differential (PID) controller. As the oven does not cover the adjacent stainless steel feedthrough, no heated metal surfaces except the catalyst surface are exposed to the reactants. Reaction temperatures up to 400 °C are possible. The temperature difference between the reactor walls and the sample inside the reactor was determined as a function of the temperature, of the rate of gas circulation, and the partial pressure of the diluting gas. If a partial pressure of He of ~1bar is used to dilute the reactants, the thermal equilibration of the catalyst with the outer wall/ oven is sufficiently fast to limit the temperature hysteresis between the outer-wall-contacted thermocouple and the sample to less than 2 degrees at a heating rate of 10K/min. The reaction temperatures given in the main paper are corrected for this offset. An all-metal circulation pump, a pressure gauge, and a sample valve are connected to the reaction cell, forming a loop with a total volume of 65 ml. Additionally, an uncoated glass capillary is inserted directly into the cell to measure the partial pressures of reactants and products continuously via EID/ QMS detection (not shown in the apparatus scheme but visible in the photograph). The reaction gases are introduced into the circulation system by a gas manifold and are continuously pumped through the reactor. Additionally, a sample of the reaction gas is taken with a 200 ml sample loop at the end of the reaction and analyzed by gas chromatography with mass selective detection, in order to determine the final gas phase composition after reaction.

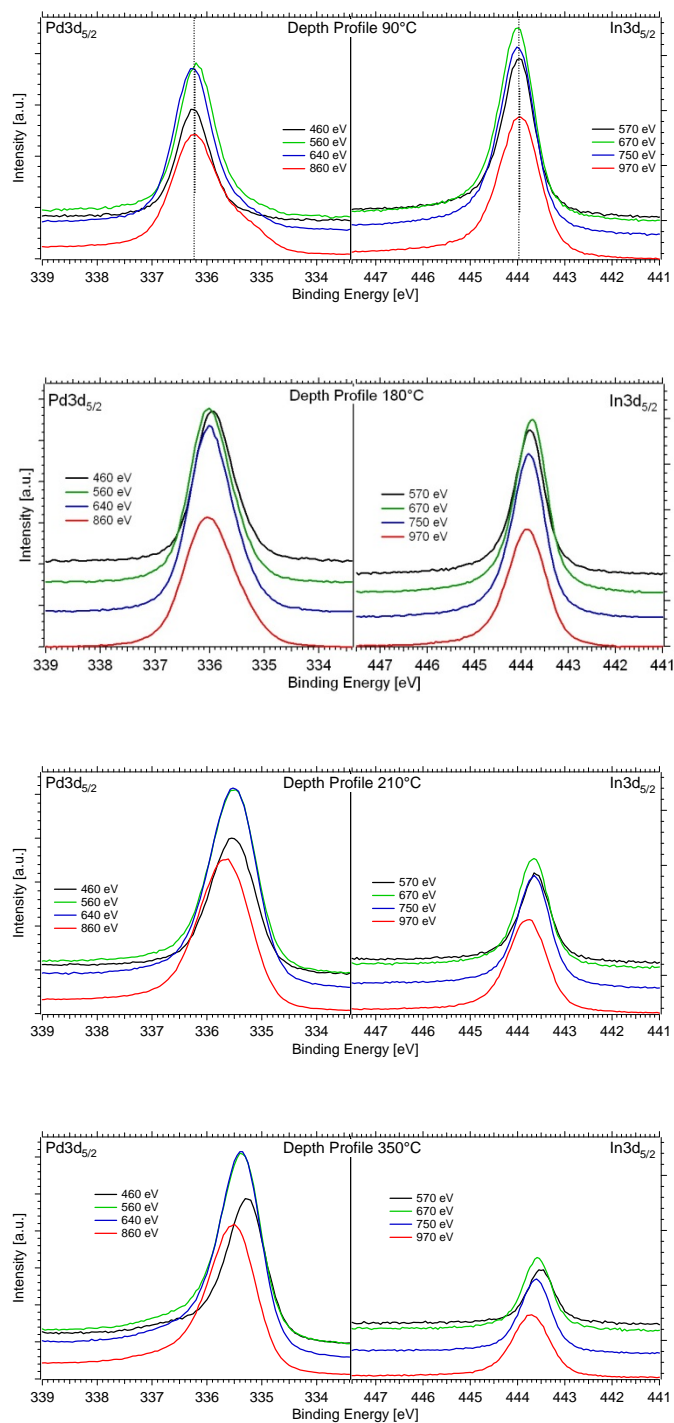


Figure S2: Depth profiling of In-metal distribution perpendicular to the surface by photon energy variation (resulting kinetic energies 570 – 670 – 750 – 970 eV, corresponding IMFP's 965 – 1075 – 1160 – 1388 pm).

Ad Figure S2: Figure S2 provides the depth profiling data that are used to set up Figure 3 of the main paper. Pd 3d_{5/2} and In 3d_{5/2} peaks are compared for four different temperatures (363 K, 453 K, 483 K and 623 K), showing that the indium concentration profile changes from In-rich conditions near the surface to a diluted state at high temperatures, explaining the XPS-observed alterations of Pd-coordination by indium.

Ad Fig. S3: Fig.S3 provides the conversion of the reaction rates of Figure 4 of the main paper (given therein as pressure change mbar per minute) to TOF values (given as frequency of product formation per site and second). The underlying idealized assumption is a structure-insensitive activity of uniform Pd₁In₁ surface sites toward CO, CO₂ and HCHO. Note that the ~ 1:1 surface composition was determined by comparing the peak areas of the In 3d_{5/2} and Pd 3d_{5/2} peaks.

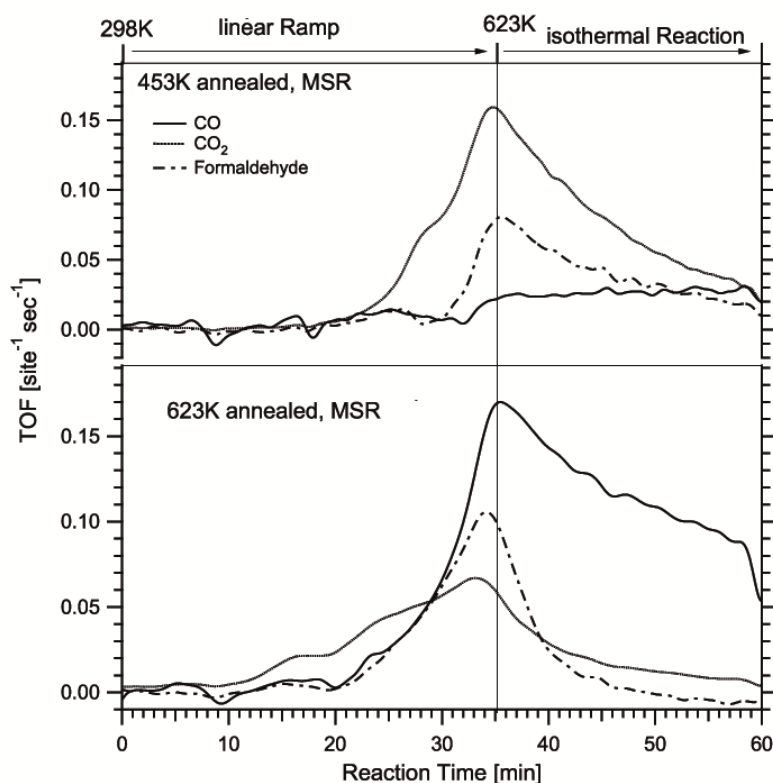


Fig. S3: TOF data corresponding to Figure 4, main text. Due to the linear temperature increase between 298K and 623K, any intermediate reaction temperature can be easily deduced by linear interpolation on the time-axis.

Ad Figs. S4 and S5: Fig. S4 and Fig.S5 provide the Figure 4-related C_1 partial product pressures and the methanol/hydrogen partial pressures, respectively, at a given reaction time and reaction temperature. The partial pressure data can e.g. be used to recalculate “true” chemical reaction rates. When there is e.g. inhibition by products with high adsorption probability, such as CO, one needs to know the dependence of rate on the concentration of both reactants and products to calculate the chemical reaction rates. In cases where products inhibit the rate, there is virtually no conversion low enough to give differential behavior and great care is needed to properly interpret the kinetic data. Thus, in absence of detailed knowledge of the pressure- and temperature-dependent kinetics, we nevertheless can provide the respective concentrations of all products and reactants in supporting Figs.S4 and S5 so one can eventually extract a rate.

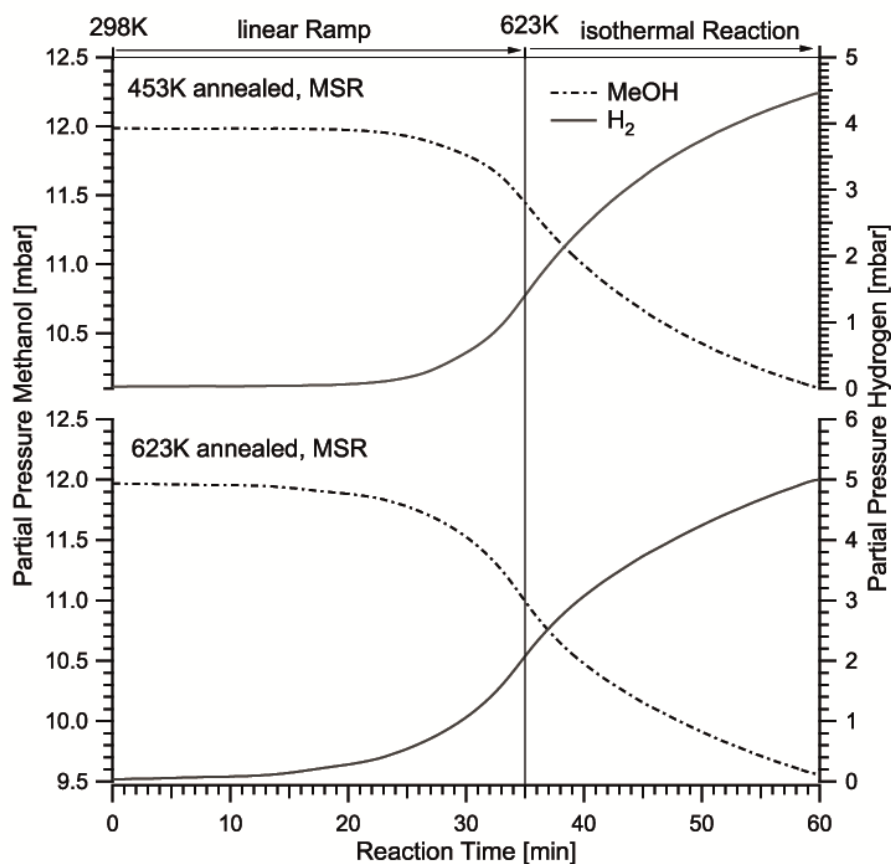


Fig. S4: Methanol and hydrogen partial pressure data corresponding to Figure 4, main text. Due to the linear temperature increase between 298K and 623K, any intermediate reaction temperature can be deduced by linear interpolation on the time-axis.

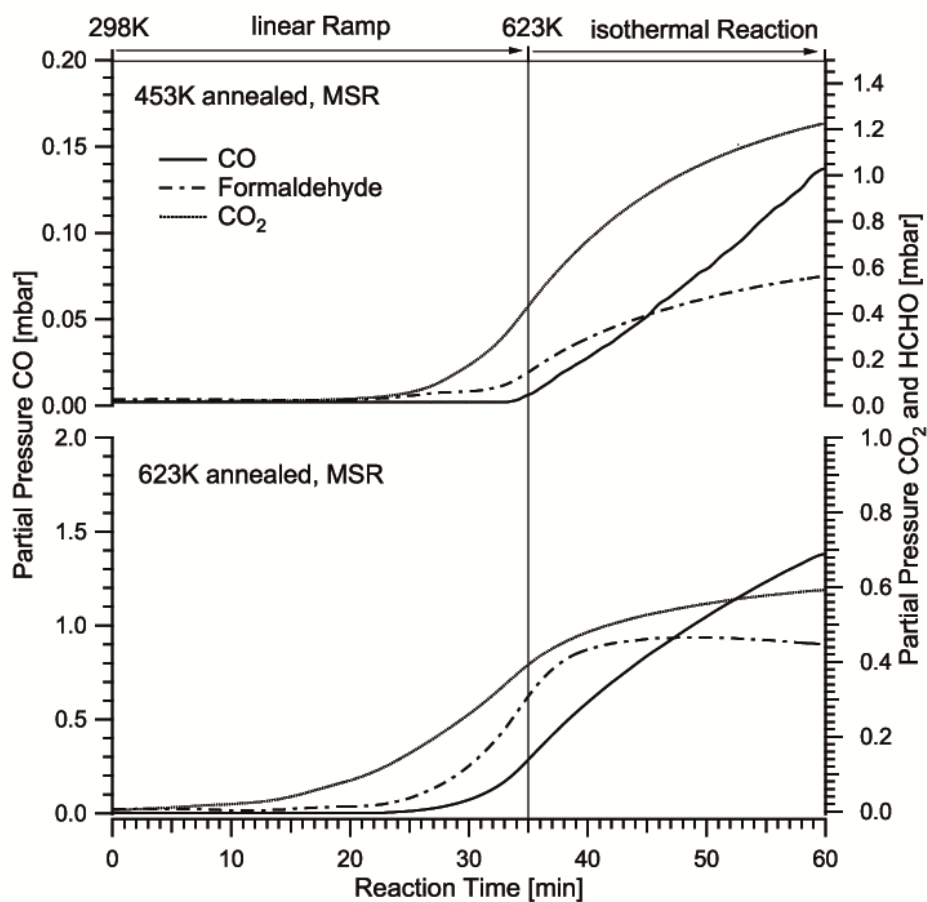


Fig. S5: C_1 partial pressure data corresponding to Figure 4, main text. Due to the linear temperature increase between 298K and 623K, any intermediate reaction temperature can be deduced by linear interpolation on the time-axis.

Fig.S6 provides the conversion of the reaction rates of Figure 7 of the main paper (given therein as pressure change mbar per minute) to TOF values (given as frequency of product formation per site and second). The underlying idealized assumption is a structure-insensitive activity of uniform Pd_1In_1 surface sites toward CO, CO_2 and HCHO.

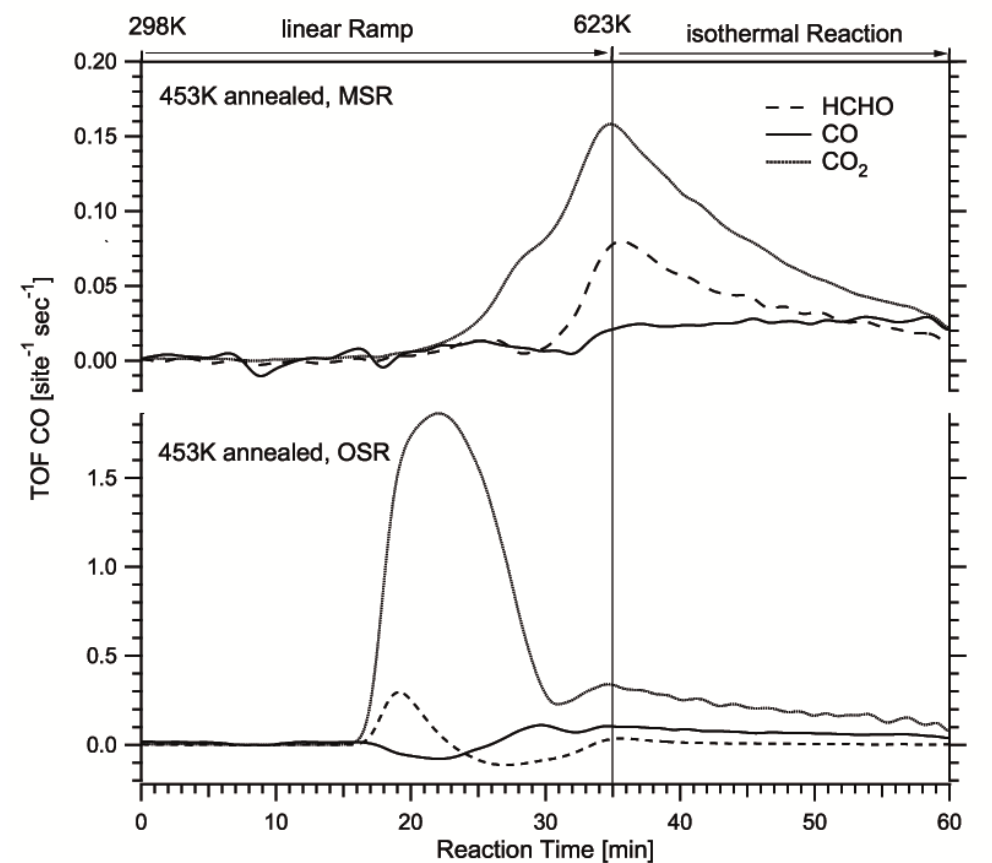


Fig. S6: TOF data corresponding to Figure 7, main text. Due to the linear temperature increase between 298K and 623K, any intermediate reaction temperature can be easily deduced by linear interpolation on the time-axis.

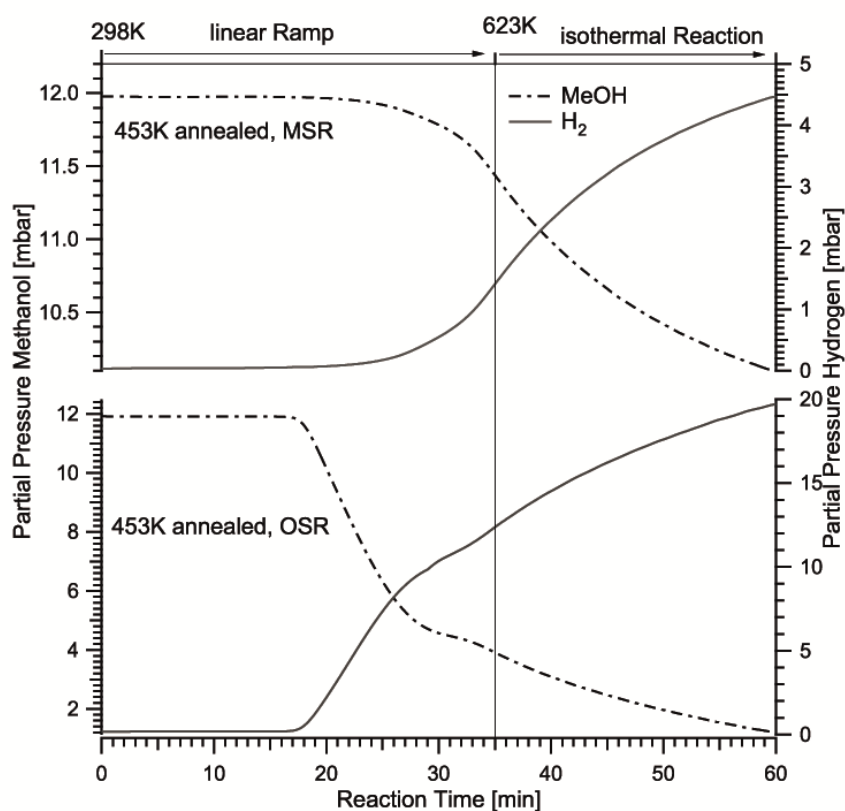


Fig. S7: Methanol and hydrogen partial pressure data corresponding to Figure 7, main text. Due to the linear temperature increase between 298K and 623K, any intermediate reaction temperature can be deduced by linear interpolation on the time-axis.

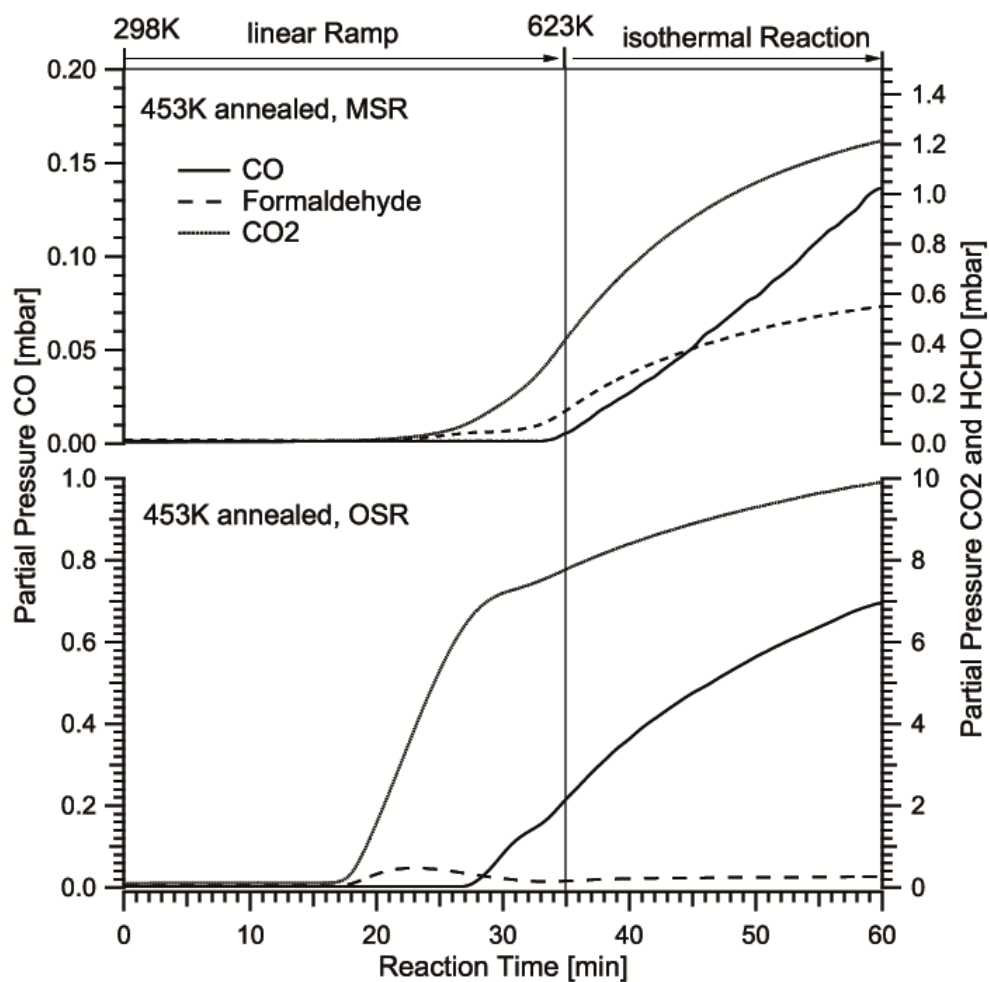


Fig. S8: C₁ partial pressure data corresponding to Figure 7, main text. Due to the linear temperature increase between 298K and 623K, any intermediate reaction temperature can be deduced by linear interpolation on the time-axis.